

Model Predictive Control with ESO And an Improved Speed Loop for PMSM

Dingdou Wen¹, Wenting Zhang¹, Zhongjian Tang¹,
Xu Zhang¹, and Zhun Cheng^{2,*}

¹Hunan University of Technology, Zhuzhou 412007, China

²Hunan Railway Professional Technology College, Zhuzhou 412001, China

ABSTRACT: An Improved Speed Loop (ISL) and Extended State Observer (ESO) strategy based on Model Predictive Control (MPC) of the Permanent Magnet Synchronous Motor (PMSM) is proposed in this paper. Firstly, considering the impact of load torque sudden changes on speed tracking performance, a reduced-order Luenberger observer is utilized to observe the load torque and combine with model prediction to form ISL. Secondly, the ESO is utilized to estimate the lumped disturbance and feedforward compensated to the improved speed loop, which improves the system's anti-interference performance. Then, a cost function that introduces the current tracking error at the switching point is constructed, reducing the current ripple. Finally, the experiments show that compared with the traditional PI speed control, the proposed strategy reduces the speed overshoot over a wide range of speeds, improves the speed tracking performance, and has superior dynamic performance and anti-disturbance performance under different operating conditions.

1. INTRODUCTION

Finite Control Set Model Predictive Current Control (FCS-MPCC), as a promising high-performance Permanent Magnet Synchronous Motor (PMSM) driving strategy, has attracted more and more attention from scholars due to its advantages such as simple structure, fast response speed, flexible design, and multi-objective synergy [1]. PMSM has been widely recognized in various industrial fields due to high power density, high efficiency, and compact structure [2]. In Model Predictive Control (MPC), the speed loop usually adopts Proportional Integral (PI) control. PI control algorithm is simple, reliable, and linear. PMSM is a multivariable and nonlinear system, which is affected by internal and external disturbances and uncertainties during the operation of the motor. Therefore, traditional PI controllers cannot achieve self-adjustment. Their dynamic response is slow; overshoot is large; robustness is poor, and they cannot meet control scenarios with high control accuracy requirements [3]. To address these shortcomings, [4] proposes using Integral Proportional (IP) to replace traditional PI speed controllers, overcoming the drawback of large overshoot of traditional PI. The effectiveness of the IP control is experimentally verified. Ref. [5] proposes a composite variable structure PI control to accelerate speed response. Although these methods can reduce speed overshoot and improve speed following performance, the system's anti-interference ability is poor. Ref. [6] designs a speed loop control based on Fast Terminal Sliding Mode Reaching Law (FTSMRL) on the super distortion algorithm, which improves the response speed and disturbance suppression ability, but its immunity to the disturbance of the super-twisting algorithm is poor. Therefore, in recent years,

many scholars have conducted further research on PMSM control and developed many nonlinear control methods, such as adaptive control [7], robust control [8], neural network control [9], sliding mode control [10], and fuzzy control [11].

Due to the neglect of load torque and unmodeled external disturbances by traditional PI speed control, sudden load changes will affect motor control performance. However, in high-performance servo systems, load disturbances have an impact on motor speed, control accuracy, speed range, and dynamic performance. Therefore, in PMSM control, load anti-interference performance must be considered. At present, there are methods for load observation, such as direct calculation method [12], model adaptation method [13], full-order and reduced-order Luenberger observers [14], and extended state observers [15]. The state observer can solve the issue of unobservable state variables, so it is a better choice to use state observer to observe load disturbances. The load torque is observed by the reduced-order Luenberger observer in this paper, and the observed values are used as input for model prediction. In other words, an Improved Speed Loop (ISL) is constructed by combining the reduced-order Luenberger observer with model prediction.

Due to the influence of load torque disturbance, parameter uncertainty, and delay on the performance of control systems, many scholars have introduced disturbance feedforward compensation in the speed loop to solve these problems. Refs. [16, 17] introduce a feedforward compensation method based on disturbance observer in the speed loop, which improves the system's anti-interference ability and robustness. However, sliding mode control is applied to both, which cannot ensure zero-error operation on the sliding mode surface and

* Corresponding author: Zhun Cheng (120277982@qq.com).

inevitably leads to system chattering. Refs. [18, 19] propose a new adaptive reaching law and combine it with a novel observer to observe the lumped disturbance of the PMSM in real time and perform feedforward compensation to further improve the perturbation suppression. A reduced-order Generalized Proportional Integral (GPI) observer is proposed in [20], and it is employed to compensate for the parameter mismatch lumped disturbance and suppressed distortion. Therefore, this paper considers designing corresponding feedforward control designs to compensate for lumped disturbances. Extended State Observer (ESO), as a disturbance estimation technique, has been introduced into PMSM control systems [21, 22]. Nowadays, its application has solved many practical engineering problems [23, 24]. Its core is to use ESO to estimate internal states and external disturbances in real time, and its practicality has also been confirmed [25, 26].

In the optimization process of MPC cost function, the current prediction tracking error term is often used as the basic term of the cost function. For single vector control, it can effectively improve the steady-state performance of the system [27]. However, for dual vector control, only considering the current prediction tracking error term will ignore the impact of switching point current error on cost function optimization, resulting in the vector combination that minimizes the cost function not being globally optimal and increasing current ripple. Therefore, in dual vector control, in order to reduce current ripple, this paper introduces switching point error in the cost function.

In summary, the model prediction is combined with the reduced-order Luenberger observer to form the ISL. ISL is feedforward compensated through ESO, and the reduced-order Luenberger observer and ESO are used to double observe and compensate for the load and lumped disturbances, which further reduces the impact of disturbance perturbation on speed tracking, resulting in faster response and smaller overshoot. The current error term of the dual vector switching point is introduced into the cost function to reduce current jitter. The contributions of this paper are as follows.

- (i) A load torque observer and an ESO are designed to improve the system's anti-interference ability.
- (ii) Compared with traditional PI, the proposed method improves fastness of the system and reduces the overshoot of speed.
- (iii) By introducing the cost function of switching point current error, the current ripple is reduced.

This paper is structured as follows. The mathematical model of PMSM is introduced in Section 2. The single cost function MPC with the introduction of a dual vector switching point current error term is proposed in Section 3. The ISL + ESO model predictive control strategy is proposed in Section 4. The effectiveness of the proposed strategy is verified through experiments in Section 5. Finally, a summary is provided in Section 6.

2. MATHEMATICAL MODEL OF PMSM

In this paper, the object of the study is the surface PMSM, assuming that the saturation of the magnetic core of the motor is ignored, not counting the turbine and magnetic stagnation loss

in the motor, and the current in the engine is symmetric to the three-phase sine wave current [28].

The stator current equation for PMSM is expressed as follows.

$$(u_d - R_s i_d + \omega_e L_s i_q) / L_s = \frac{di_d}{dt} \quad (1)$$

$$(u_q - R_s i_q - \omega_e L_s i_d - \omega_e \psi_f) / L_s = \frac{di_q}{dt} \quad (2)$$

where R_s is the stator resistance; ψ_f is the permanent magnet flux linkage; L_s is the stator inductance; ω_e is the electrical angular velocity; u_d and u_q are the d - q axis voltage, respectively; i_d and i_q are the d - q axis current, respectively.

Equations (1) and (2) can be described by first-order Eulerian, and the equations are as follows:

$$i_d(k) + T_s [u_d(k) - R_s i_d(k) + e_d(k)] / L_s = i_d(k + 1) \quad (3)$$

$$e_d(k) = \omega_e(k) L_s i_q(k) \quad (4)$$

$$i_q(k) + T_s [u_q(k) - R_s i_q(k) + e_q(k)] / L_s = i_q(k + 1) \quad (5)$$

$$e_q(k) = -\omega_e(k) L_s i_d(k) - \omega_e(k) \psi_f \quad (6)$$

where T_s is the sampling time; $e_d(k)$ and $e_q(k)$ are the d - q axis back EMF at instant k , respectively; $i_d(k)$ and $i_q(k)$ are the d - q axis current at instant k , respectively; $i_d(k + 1)$ and $i_q(k + 1)$ are the d - q axis current at instant $k + 1$, respectively.

3. DUAL-VECTOR MPC WITH IMPROVED COST FUNCTION

There are 8 voltage vectors in 2L-VSL, namely: six effective voltages and two zero vectors, and 49 combinations of two voltage vectors can be synthesized, but the computational complexity is relatively high. This paper designs each section using a combination of 1 effective vector and 1 zero vector or 2 effective vectors. The principle of dead-beat is adopted, and the time for two voltage vectors to operate in one sampling period is allocated on the q -axis. The sequence of two vectors in a sampling cycle does not affect the working time of the vectors, so the optimal combination only needs to be selected from 21 combinations of pairwise voltage vectors.

Assuming that the first vector is selected as V_4 , it needs to be combined with V_0 , V_5 , and V_6 respectively and assigned the action time, as shown in Fig. 1. From Fig. 1, it can be seen that at the end of the control cycle, there is almost no error between the reference current and the predicted current at instant $(k + 1)$, so the current error term at the dual vector switching point can well reflect the current ripple in the entire control cycle. In traditional cost functions, only the current tracking effect at the end of a control cycle is valued, while the current ripple at the vector switching point is ignored. To ensure that the chosen vector combination is the global optimal and has less fluctuation, the current error term of the vector switching point is introduced into the cost function.

The duty cycle is calculated using the q -axis current deadbeat method. Namely, in one sampling cycle, by assigning the time of action of the two voltage vectors (V_i and V_j), $i_q(k + 1)$ is equal to i_q^* at instant $k + 1$, i.e.:

$$i_q(k + 1) = i_q^* = i_q(k) + s_i T_i + s_j (T_s - T_i) \quad (7)$$

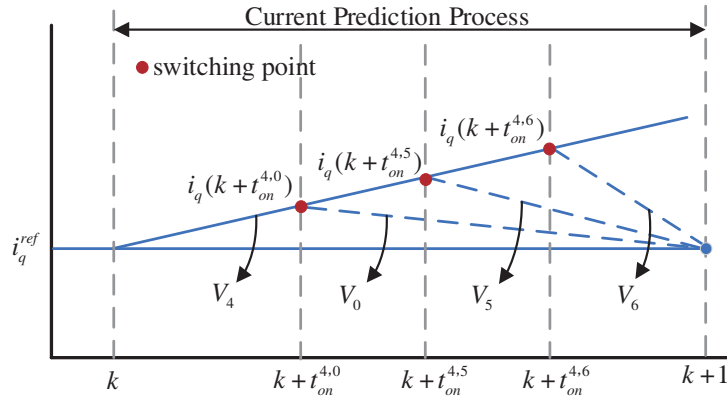


FIGURE 1. Dual-vector prediction process.

where s_i and s_j are the rate of change of i_q at the action of the first vector and the rate of change of i_q at the action second vector, respectively.

According to (7), the voltage vector switching point time can be obtained:

$$T_i = [i_q^* - i_q(k) - s_j T_s] / (s_i - s_j) \quad (8)$$

Define $t_i = T_i / T_s$, and then $k + t_i$ denotes the dual vector switching point moment. Based on the switching point time and $i_d(k)$, $i_q(k)$, and Equations (3) and (4), the predicted current values $i_d(k + t_i)$ and $i_q(k + t_i)$ at the switching point can be obtained. The expression is as follows:

$$i_d(k + t_i) = i_d(k) + T_i [u_{di}(k) - R_s i_d(k) + e_d(k)] / L_d \quad (9)$$

$$i_q(k + t_i) = i_q(k) + T_i [u_{qi}(k) - R_s i_q(k) + e_q(k)] / L_q \quad (10)$$

Similarly, considering the influence of the action time of the first vector in the vector combination on the predicted current value at instant $k+1$, the predicted value of the stator current at the next instant can be obtained from Equations (3) and (4) for $i_d(k+1)$ and $i_q(k+1)$. The equations are as follows

$$i_d(k+1) = i_d(k) + \frac{T_i}{L_d} u_{di}(k) + \frac{T_s - T_i}{L_d} u_{dj}(k) + \frac{T_s}{L_d} [-R_s i_d(k) + e_d(k)] / L_d \quad (11)$$

$$i_q(k+1) = i_q(k) + \frac{T_i}{L_q} u_{qi}(k) + \frac{T_s - T_i}{L_q} u_{qj}(k) + \frac{T_s}{L_q} [-R_s i_q(k) + e_q(k)] / L_q \quad (12)$$

The traditional cost function g_1 is as follows:

$$g_1 = |i_q^* - i_q(k+1)|^2 + |i_d^* - i_d(k+1)|^2 + \lambda(2*|S_1^k - S_2^k| + |S_1^k - S_2^{k-1}|) \quad (13)$$

As shown in Fig. 1, the current tracking error at the vector switching point can reflect the current ripple in the entire control cycle. At the same time, considering that multiple non-linear control objectives can be taken into the cost function, it is necessary to construct a novel cost function that introduces both the current error at the switching point and the switching

frequency of the converter. Due to the consideration of switching point current error and current prediction error, the current error is smaller when the cost function is optimized, and the current ripple is further reduced by the current loop. Finally, the predicted current values obtained are sequentially brought into the cost function, and the combination of voltage vectors that minimizes the value of the cost function is selected.

Because the current error at the switching point has the same dimension as the stator current tracking error, no weight coefficient is required. However, the number of switch changes is different from the dimension of the current, and a weight coefficient λ needs to be designed. The novel cost function constructed is as follows:

$$g_2 = |i_q^* - i_q(k + t_i)|^2 + |i_d^* - i_d(k + t_i)|^2 + |i_q^* - i_q(k+1)|^2 + |i_d^* - i_d(k+1)|^2 + \lambda(2*|S_1^k - S_2^k| + |S_1^k - S_2^{k-1}|) \quad (14)$$

where S_2^{k-1} is the last switch sequence of the vector combination selected for the past control cycle. S_1^k and S_2^k are the first and second vector switching states for the voltage vector combination selected in the current control cycle.

4. DESIGN OF ISL + ESO

4.1. Improved Design of Speed Loop

(1) Determination of the given value i_q^*

Under the dual vector control strategy of $i_d = 0$, the mechanical motion equation and torque equation of PMSM can be simplified as follows:

$$T_e = \frac{3}{2} p \psi_f i_q \quad (15)$$

$$J \frac{d\omega_m}{dt} = T_e - T_L - B \omega_m \quad (16)$$

where ω_m is the mechanical angular velocity; p is the number of pole pairs; J is the moment of inertia; T_e is electromagnetic torque; T_L is the load torque; B is the damping coefficient.

From Equations (15) and (16), the following expressions can be obtained:

$$\frac{d\omega_m}{dt} = \frac{3}{2J} p \psi_f i_q - \frac{1}{J} T_L - \frac{B}{J} \omega_m \quad (17)$$

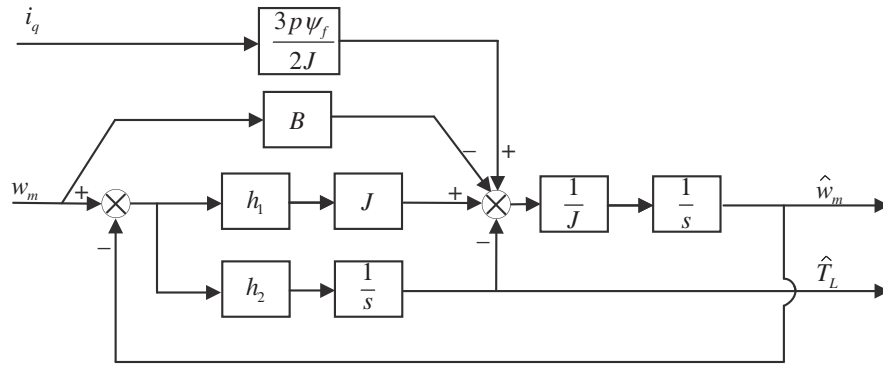


FIGURE 2. The block diagram of the reduced-order Luenberger observer.

Taking the derivative of Equation (17), the following equation is obtained:

$$\frac{d^2\omega_m}{dt^2} = \frac{3}{2J}p\psi_f \frac{di_q}{dt} - \frac{1}{J} \frac{dT_L}{dt} - \frac{B}{J} \frac{d\omega_m}{dt} \quad (18)$$

By performing Taylor discretization on equation (18) and omitting quadratic and above terms, it can be obtained that:

$$\omega_m(k+1) = \omega_m(k) + T_{sw} \cdot \dot{\omega}_m|_k + \frac{T_{sw}^2}{2} \cdot \ddot{\omega}_m|_k \quad (19)$$

where T_{sw} is the sampling period of the speed control loop.

A first-order Eulerian discretization is applied to i_q , and the following equation can be obtained:

$$\frac{di_q}{dt} = \frac{i_q(k+1) - i_q(k)}{T_{sw}} \quad (20)$$

According to the principle of dead-beat, it can be obtained that $i_q(k+1) = i_q^*$ and $w_m(k+1) = w_m^*$, and the load torque remains constant during the sampling period, where i_q^* and w_m^* are the given values of the q -axis stator current and mechanical angular velocity, respectively.

Bringing Equations (15), (16), (17), (18), and (20) into Equation (19), the reference current of the q -axis stator is as:

$$i_q^* = -\frac{1}{J^2 K_T T_{sw}} (2J^2 \omega_m^k - 2J^2 \omega_m^* + B^2 T_s^2 \omega_m^k + B_m \hat{T}_L T_{sw}^2 p - 2B J T_{sw} \omega_m^k - 2J \hat{T}_L T_{sw} p + i_q^k J^2 K_T T_{sw} - B i_q^k J K_T T_{sw}^2) \quad (21)$$

where $K_T = \frac{3p^2\psi_f}{2J}$, and \hat{T}_L is the estimated value of load torque, which is obtained by using the reduced-order Luenberger observer.

(2) Design of Load Torque Observation based on reduced-order Luenberger observer

In the full-order Luenberger observer, the rotor position, speed, and torque are used as the state variables of the observer, which requires consideration of the selection of three expected pole positions, and the debugging process is cumbersome. Therefore, in this paper, a reduced-order Luenberger observer is designed, which has a simple structure, easy to solve

the gain matrix, and easy to implement. The designed reduced-order Luenberger observer takes i_q as the input variable, w_m as the output variable, and \hat{w}_m and \hat{T}_L as the state variables. Equation (17) is rewritten as:

$$\begin{cases} \frac{d\omega_m}{dt} = -\frac{B}{J}\omega_m - \frac{1}{J}\hat{T}_L + \frac{3p\psi_f}{2J}i_q + h_1(\omega_m - \hat{\omega}_m) \\ \frac{d\hat{T}_L}{dt} = h_2(\omega_m - \hat{\omega}_m) \end{cases} \quad (22)$$

Equation (22) is rewritten as the state equation of the Luenberger observer:

$$\begin{cases} \dot{\hat{x}} = A\hat{x} + Bu + H(y - \hat{y}) \\ \hat{y} = C\hat{x} \end{cases} \quad (23)$$

where $\hat{}$ represents the estimated value, and $A =$

$$\begin{bmatrix} -\frac{B}{J} & -\frac{1}{J} \\ 0 & 0 \end{bmatrix}, B = \begin{bmatrix} \frac{3p\psi_f}{2J} \\ 0 \end{bmatrix}, C = [10], H = \begin{bmatrix} h_1 \\ h_2 \end{bmatrix},$$

$$\hat{x} = \begin{bmatrix} \hat{\omega}_m \\ \hat{T}_L \end{bmatrix}, u = i_q.$$

Figure 2 shows the block diagram of the reduced-order Luenberger observer.

The actual model's state equation is as follows:

$$\begin{cases} \dot{x} = Ax + Bu \\ y = Cx \end{cases} \quad (24)$$

The error equation of state for the state observer is given by subtracting both sides of Equation (22) and Equation (24) correspondingly as:

$$\dot{e} = (A - HC)e \quad (25)$$

where e is the state estimation error ($e = x - \hat{x}$).

The characteristic equation of Equation (25) is as:

$$\det[sI - (A - HC)] = s^2 + \left(h_1 + \frac{B}{J}\right)s - \frac{1}{J}h_2 = 0 \quad (26)$$

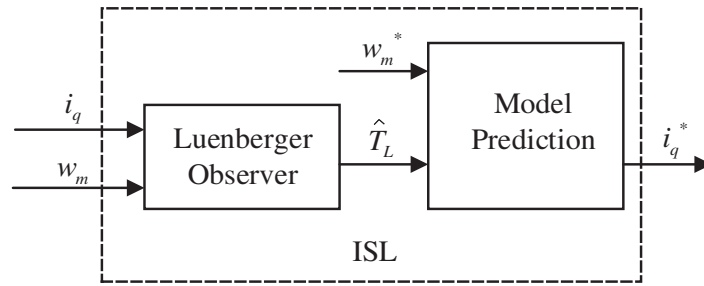


FIGURE 3. The block diagram of ISL.

If the expected poles are p_1 and p_2 , respectively, Equation (26) can be written as $(s - p_1)(s - p_2) = 0$, and it can be obtained that:

$$\begin{cases} h_1 = -p_1 - p_2 - B/J \\ h_2 = -Jp_1p_2 \end{cases} \quad (27)$$

Discretizing Equation (22), the recursive formula for the rotational speed and load observations is as follows:

$$\begin{cases} \hat{\omega}_m(k+1) = (1 - T_{sw}h_1)\hat{\omega}_m(k) + T_{sw} \left(h_1 - \frac{B}{J} \right) \omega_m(k) \\ \quad + \frac{3T_{sw}}{2J} p\psi_f i_q(k) - \frac{T_{sw}}{J} \hat{T}_L(k) \\ \hat{T}_L(k+1) = \hat{T}_L(k) + T_{sw}h_2[\omega_m(k) - \hat{\omega}_m(k)] \end{cases} \quad (28)$$

4.2. Control Strategy Based on ISL + ESO

ESO is used to perform feedforward compensation for the total disturbance to improve the anti-interference performance of ISL. Considering motor parameter perturbations and load disturbances, Equation (17) is rewritten as:

$$\dot{w} = (a + \Delta a)i_q - (b + \Delta b)w - (c + \Delta c)T_L \quad (29)$$

where $a = 3p\psi_f/2J$, $b = B/J$, $c = 1/J$. Δa , Δb , and Δc are parameter perturbations, respectively.

Let:

$$d(t) = \Delta a i_q - \Delta b w - (c + \Delta c)T_L + a(i_q - i_q^*) \quad (30)$$

where $d(t)$ represents the total disturbance, including external load disturbance, q -axis current tracking error, etc.

Rewrite Equation (29) as:

$$\dot{w} = a i_q^* - b w + d(t) \quad (31)$$

Let $x_1 = w$, $x_2 = d(t)$, and Equation (31) can be expressed as follows:

$$\begin{cases} \dot{x}_1 = x_2 + a i_q^* - b x_1 \\ \dot{x}_2 = c(t) \end{cases} \quad (32)$$

According to [29], the second-order extended state observer constructed is as follows:

$$\begin{cases} \dot{z}_1 = z_2 + a i_q^* - b x_1 - \beta_1 \text{fal}(e, \alpha, \delta) \\ \dot{z}_2 = -\beta_2 \text{fal}(e, \alpha, \delta) \end{cases} \quad (33)$$

where z_1 is the estimated motor speed; z_2 is the estimated motor disturbance; $e = z_1 - x_1$, and the nonlinear function $\text{fal}(e, \alpha, \delta)$ is as follows:

$$\text{fal}(e, \alpha, \delta) = \begin{cases} \frac{e}{\delta^{1-\alpha}} & |e| \leq \delta \\ |e|^\alpha \text{sign}(e) & |e| > \delta \end{cases} \quad (34)$$

where δ is the filter factor, and α is the nonlinear factor, $0 < \alpha < 1$.

Figure 3 shows the block diagram of the improved speed loop.

When the ESO converges, the lumped disturbance can be obtained, and the q -axis current \hat{i}_q^* corresponding to the total disturbance can be calculated from Equation (34), which is feedforward to the speed loop to compensate for the disturbance.

$$\hat{i}_q^* = -\frac{z_2}{a} \quad (35)$$

Instantaneous estimation and compensation of system lumped disturbance through ESO facilitates feedback control and improves regulation ability. Figure 4 shows the structural diagram of PMSM based on ISL + ESO composite control.

5. EXPERIMENTAL VERIFICATION

Experimental comparison of ISL + ESO controls with traditional PI control verifies the accuracy and effectiveness of the ISL + ESO method proposed. In order to achieve the hardware in the loop system of the PMSM drive system, a simulink simulation model is constructed and transferred to RT-LAB (OP5600). The controller adopts TMS320F2812. The principle figure of the RT-LAB hardware in the loop system is shown in Figure 5(a), and experimental platform of the RT-LAB is shown in Figure 5(b). Table 1 shows the PMSM parameters.

In order to verify the motor speed tracking performance, wide speed domain stable operation and anti-disturbance ability of the traditional method PI and the proposed method ISL + ESO in the motor startup and dynamic process, two experimental groups are set up: (i) traditional PI control, where $k_i = 100$ and $k_p = 0.15$. (ii) ISL + ESO control. The weight coefficients of the cost function g in two sets of experiments λ both are 0.05 and controlled with $i_d^* = 0$.

1) Dynamic performance

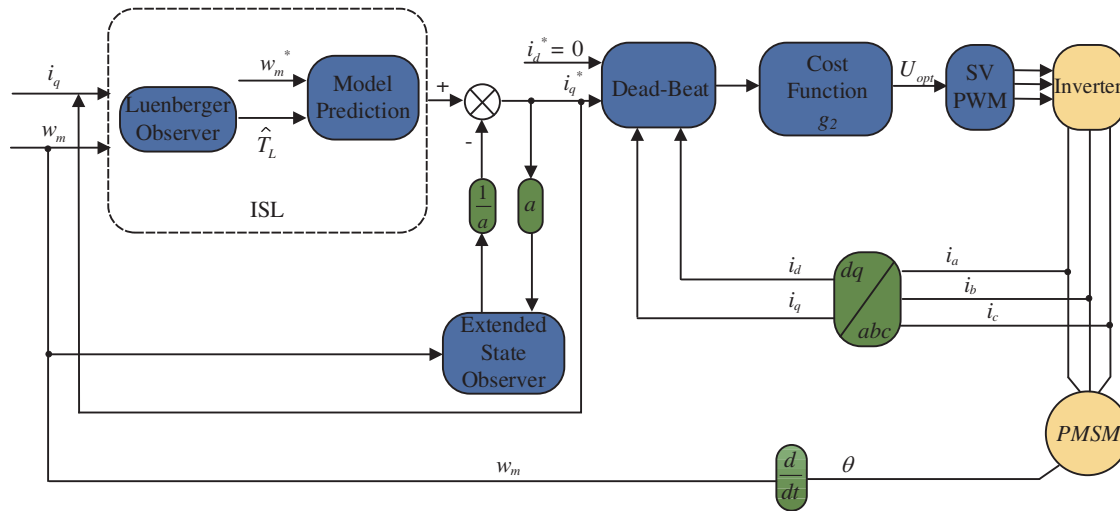


FIGURE 4. The structural diagram of PMSM based on ISL + ESO composite control.

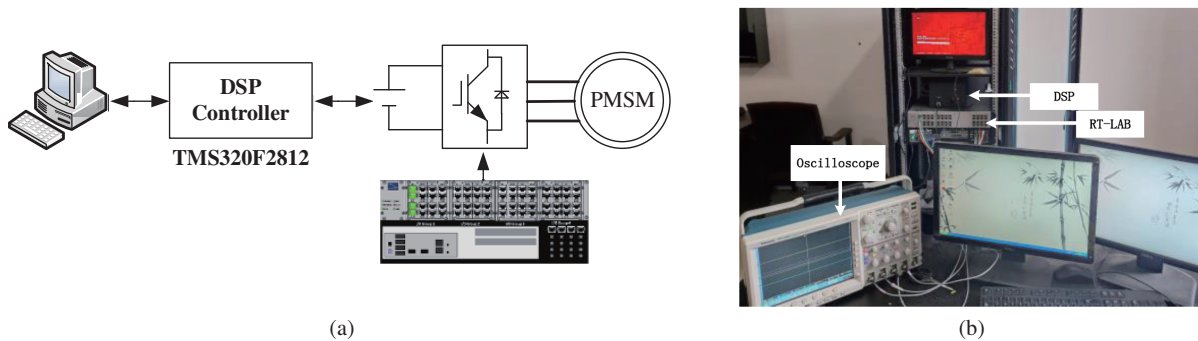


FIGURE 5. Experiment platform.

TABLE 1. The PMSM parameters.

Parameter	Value
Rated speed (r/min)	1500
Stator inductance (mH)	8.5
Permanent magnet flux (Wb)	0.24
Rated voltage (V)	311
Stator resistance (Ω)	0.2
Rated current (A)	9.4
Number of pole pairs	4
Moment of inertia ($\text{g}\cdot\text{cm}^2$)	0.00012

(1) Condition 1: no-load operation, sudden load 5 N·m at 0.2 s

In order to verify that the proposed strategy has good steady-state performance and small overshoot in a wide speed range, comparative experiments are conducted at different given speeds. The results of the overshoot and drop comparison table are shown in Table 2 (The overshoot of the no-load start speed is δ_1 . The speed drop caused by sudden load application is δ_2 . Speed reference value is w^*), and the line graph is shown in Figure 6.

Comparing 500 r/min, 1000 r/min, and 1800 r/min as representatives of low, medium, and high speeds, Figures 7(a), 8(a),

and 9(a) show the speed waveforms of traditional PI control strategies. Figures 7(b), 8(b), and 9(b) show the speed waveforms of the ISL + ESO control strategy.

From Figure 7(a), Figure 8(a), and Figure 9(a), the speed overshoot of no-load start is 12 r/min, 12.1 r/min, and 11.5 r/min, respectively. The speed drop during loading is 15.8 r/min, 15.9 r/min, and 41.2 r/min. From Figure 7(b), Figure 8(b), and Figure 9(b), the speed overshoot of no-load start is 5.8 r/min, 4.6 r/min, and 4.6 r/min, respectively. When loading, the drop in speed is 9.7 r/min, 9.7 r/min, and 38 r/min.

In summary, the proposed strategy ISL + ESO has a smaller overshoot and drops at different given speeds compared to tra-

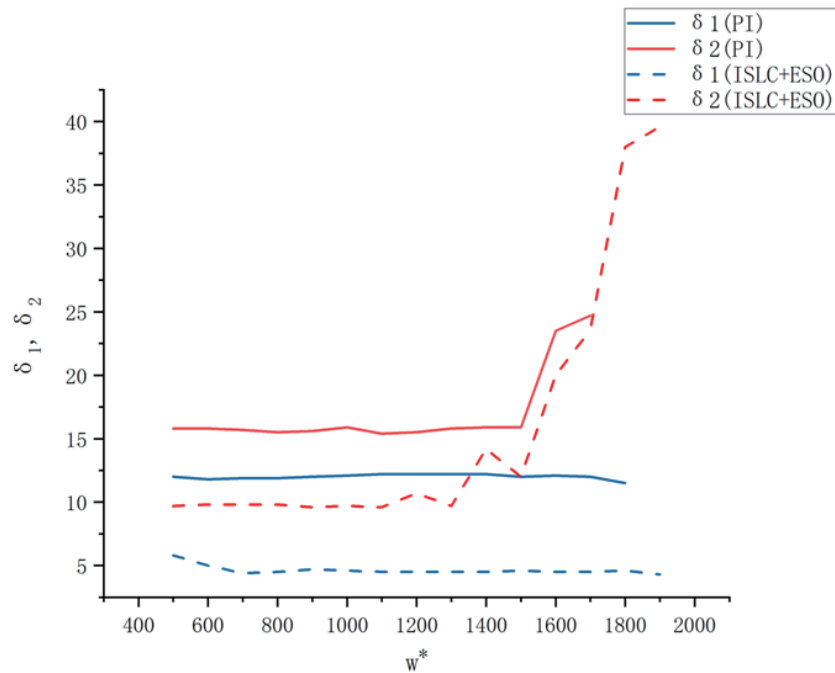


FIGURE 6. Line chart of overshoot and drop for a given speed.

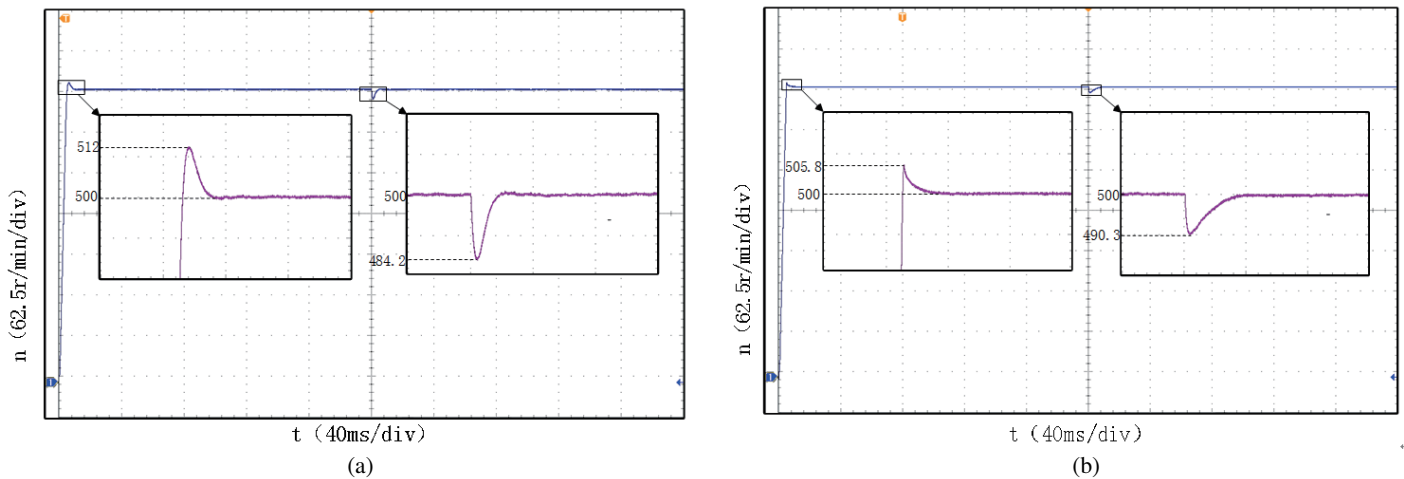


FIGURE 7. Waveform with given speed 500 r/min. (a) PI, (b) ISL + ESO.

ditional PI control. Moreover, the proposed strategy can still maintain stable speed at 1900 r/min, while the PI control exhibits oscillations in the speed waveform during sudden load application at 1800 r/min. The experimental results show that the performance of the proposed method is superior to traditional PI control.

(2) Condition 2: No-load operation, increasing to 10 N•m at 0.1 s and suddenly decreasing to 5 N•m at 0.2 s.

The dynamic performance of the two can be further compared by loading and reducing the load on the motor. Figure 10 shows the T_e waveform, and Table 3 shows the experimental data (δ and Δ respectively represent the ripple and error of T_e). From Figure 10 and Table 3, compared with the PI method, the torque ripple of the ISL + ESO method in the speed loop is

reduced by 59.1% and 53.6% when the motor is loaded and unloaded, respectively. By analyzing the experimental results, it is obtained that the ISL + ESO method has faster response and stronger anti-interference performance.

2) Steady state performance

The motor is running at no load, and the sudden load is 5 N•m at 0.2 s. The harmonic analysis of phase current i_a is shown in Figure 11. The harmonic content of the speed loop controlled by ISL + ESO and traditional PI is 6.93% and 7.8%, respectively. Compared to PI, the harmonic content of ISL + ESO is reduced by 11.1%. By analyzing the experimental results, it is obtained that the ISL + ESO control method can reduce current harmonics and current distortion.

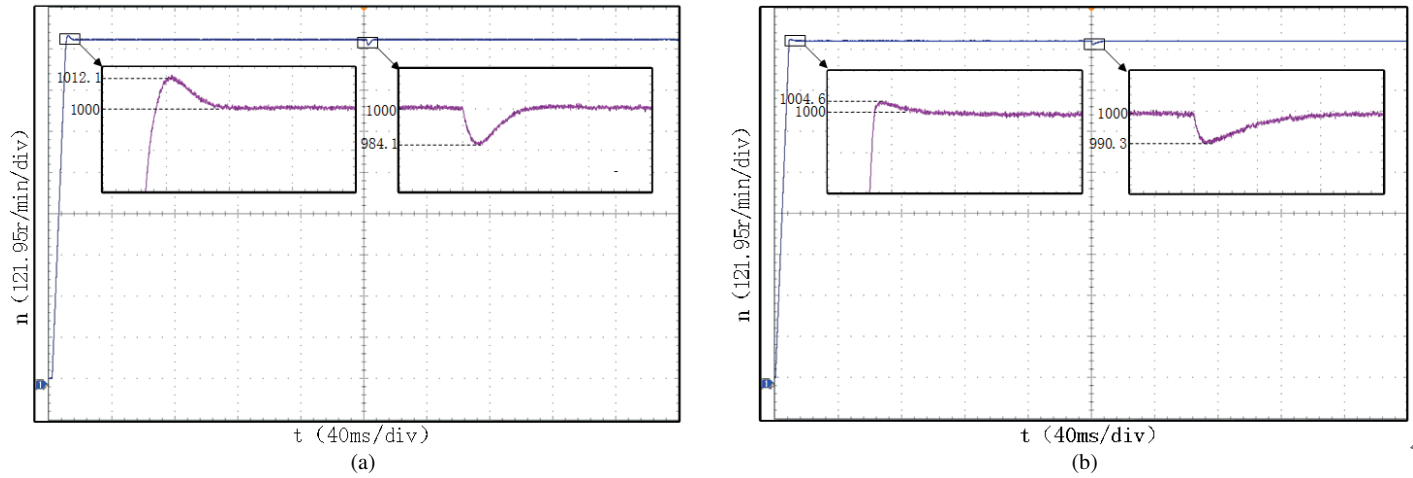


FIGURE 8. Waveform with given speed 1000 r/min. (a) PI, (b) ISL + ESO.

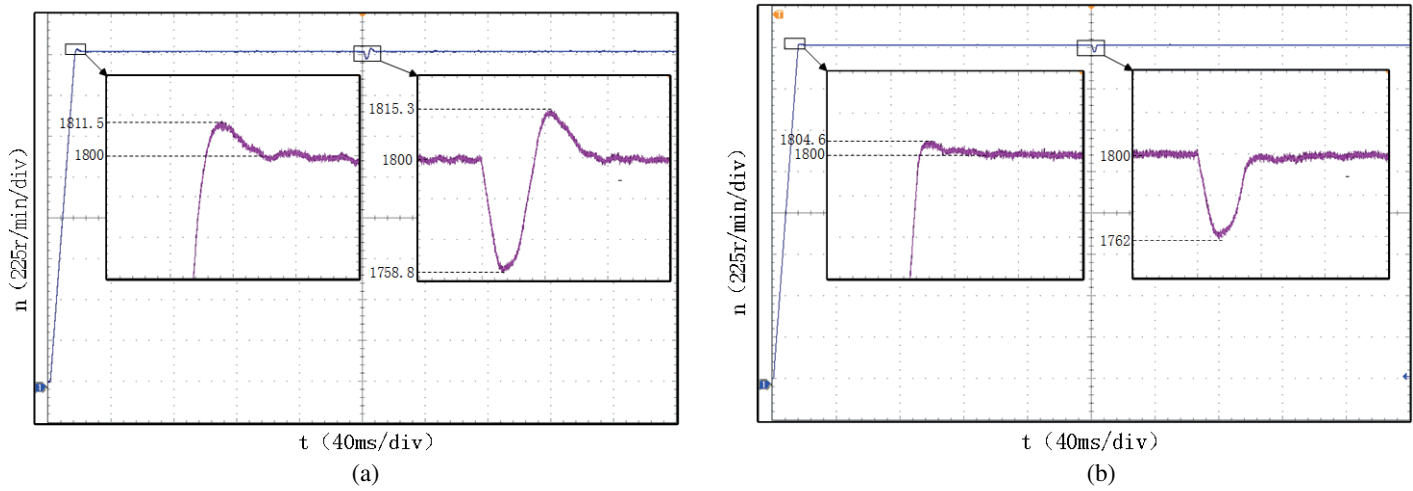


FIGURE 9. Waveform with given speed 1800 r/min. (a) PI, (b) ISL + ESO.

TABLE 2. Comparison table of the amount of overshoot and fall for a given rotational speed.

w^*	$\delta 1(\text{PI})$	$\delta 2(\text{PI})$	$\delta 1(\text{ISL} + \text{ESO})$	$\delta 2(\text{ISL} + \text{ESO})$
500	12.0	15.8	5.8	9.7
600	11.8	15.8	5.0	9.8
700	11.9	15.7	4.4	9.8
800	11.9	15.5	4.5	9.8
900	12.2	15.6	4.7	9.6
1000	12.1	15.9	4.6	9.7
1100	12.2	15.4	4.5	9.6
1200	12.2	15.5	4.5	10.7
1300	12.2	15.8	4.5	9.7
1400	12.2	15.9	4.5	14.2
1500	12.0	15.9	4.6	12.0
1600	12.1	23.5	4.5	20.0
1700	12.0	24.7	4.5	23.6
1800	11.5	oscillating	4.6	38.0
1900	continuous oscillation	continuous oscillation	4.3	39.6

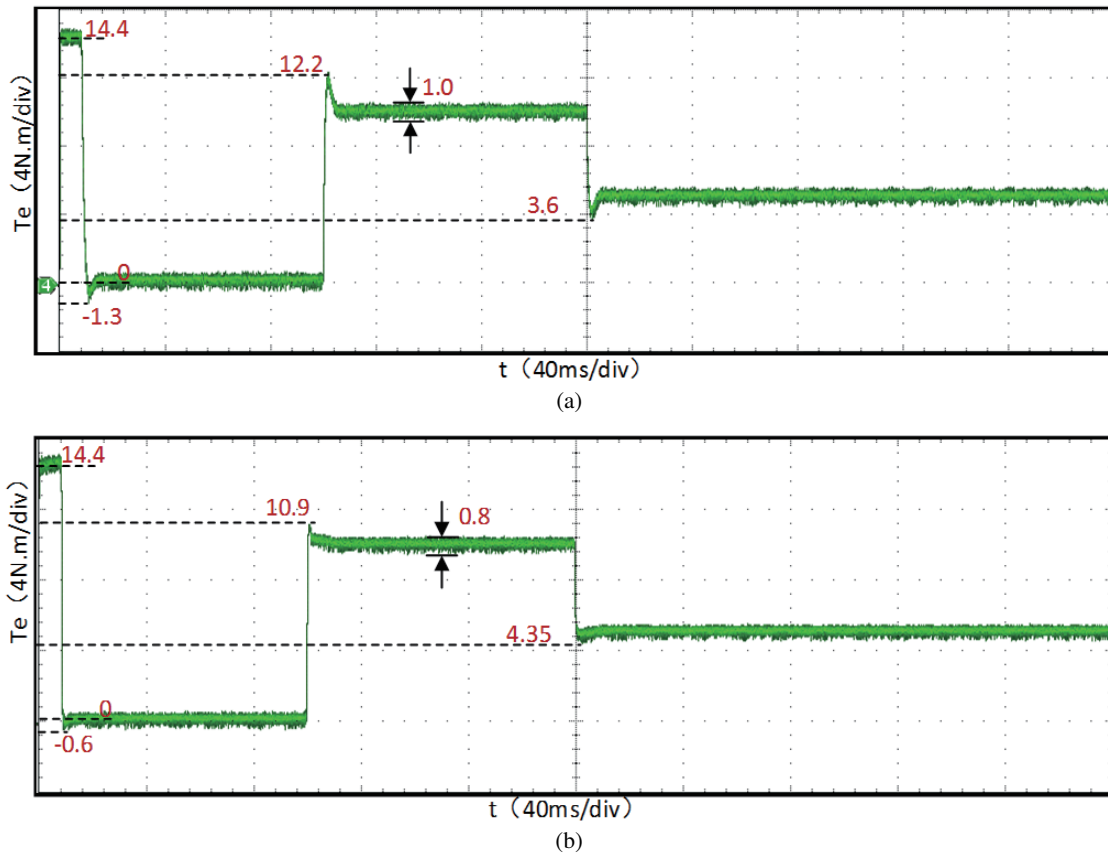


FIGURE 10. Torque waveform for loading and unloading. (a) PI, (b) ISL + ESO.

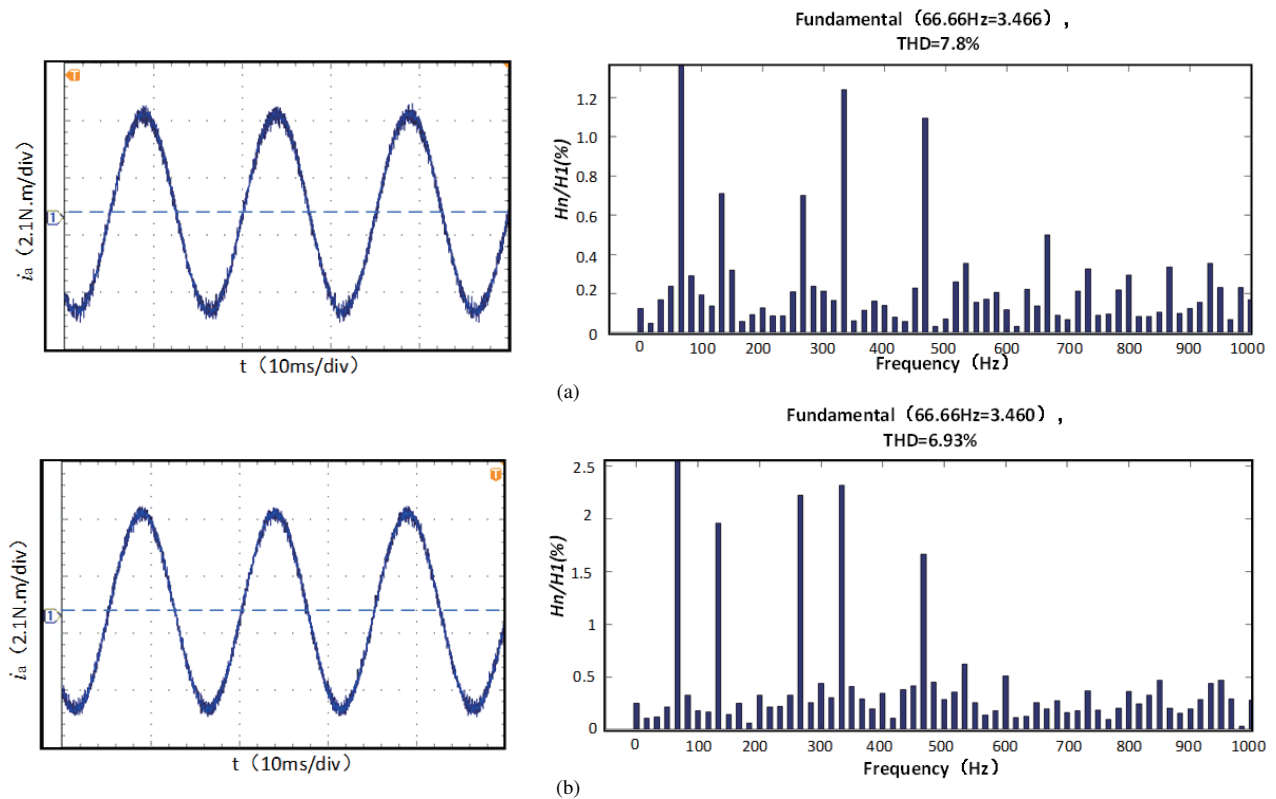


FIGURE 11. Phase current i_a waveform and FFT analysis. (a) PI, (b) ISL + ESO.

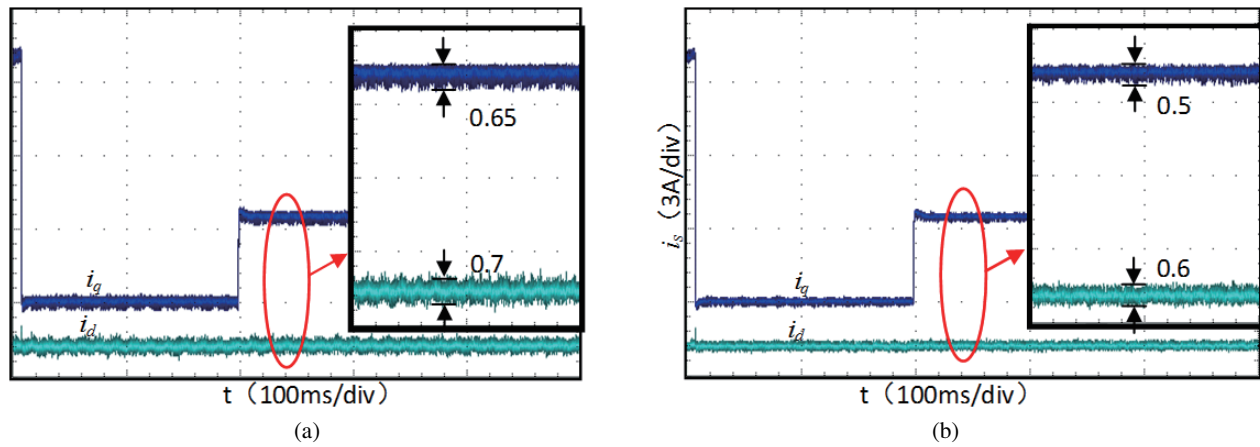


FIGURE 12. Stator current waveform. (a) g_1 , (b) g_2 .

TABLE 3. T_e comparison of two control strategies.

	PI	ISL + ESO
$0.1s\delta$ (N·m)	2.2	0.9
$0.2s\delta$ (N·m)	1.4	0.65
Δ (N·m)	1	0.8

To verify that the current ripple can be reduced by introducing the switching point current error term in the cost function, two experimental groups are designed: (i) the traditional cost function adopts g_1 ; (ii) the improved cost function adopts g_2 . Both groups of experiments are controlled by ISL + ESO with weight coefficients λ both being 0.05.

The stator current waveform of the motor running at no load and suddenly increasing to $5 \text{ N}\cdot\text{m}$ at 0.2 s is shown in Figure 12. From Figure 12, after sudden loading, the i_q and i_d current ripples using g_1 are 0.65 A and 0.7 A , respectively, while those using g_2 are 0.5 A and 0.6 A , respectively. Compared with using g_1 , the i_q and i_d ripples of g_2 method are reduced by 23.1% and 14.3%, respectively. The experimental results indicate that using the cost function g_2 method can significantly reduce current ripple and improve system performance.

6. CONCLUSION

An ESO based ISL control strategy is proposed, which uses MPC based on reduced-order Luenberger observer to improve the speed loop in this paper. By estimating the lumped disturbance through ESO, the speed loop is feedforward compensated, improving the speed tracking performance and enhancing the system's anti-interference ability. The following conclusions were obtained by analyzing the experimental results:

(1) The proposed strategy ISL + ESO effectively reduces overshoot and drops during motor startup and loading.

(2) Compared with traditional PI, the proposed strategy ISL + ESO has better dynamic performance and effectively suppresses current harmonics and torque ripple.

(3) The improved cost function g_2 effectively reduces current ripple.

ACKNOWLEDGEMENT

This work is supported by the Scientific Research Fund of Hunan Provincial Education Department under Grant Number 23B1017.

REFERENCES

- [1] Lyu, Z., X. Wu, J. Gao, and G. Tan, "An improved finite-control-set model predictive current control for IPMSM under model parameter mismatches," *Energies*, Vol. 14, No. 19, 6342, 2021.
- [2] Li, L., J. Xiao, Y. Zhao, K. Liu, X. Peng, H. Luan, and K. Li, "Robust position anti-interference control for PMSM servo system with uncertain disturbance," *CES Transactions on Electrical Machines and Systems*, Vol. 4, No. 2, 151–160, 2020.
- [3] Tursini, M., F. Parasiliti, and D. Zhang, "Real-time gain tuning of PI controllers for high-performance PMSM drives," *IEEE Transactions on Industry Applications*, Vol. 38, No. 4, 1018–1026, 2002.
- [4] Sreekumar, T. and K. S. Jiji, "Comparison of Proportional-Integral (PI) and Integral-Proportional (IP) controllers for speed control in vector controlled induction Motor drive," in *2012 2nd International Conference on Power, Control and Embedded Systems*, 1–6, IEEE, 2012.
- [5] Feng, W., J. Bai, Z. Zhang, and J. Zhang, "A composite variable structure PI controller for sensorless speed control systems of IPMSM," *Energies*, Vol. 15, No. 21, 8292, 2022.
- [6] Zhang, L., S. Wang, and J. Bai, "Fast-super-twisting sliding mode speed loop control of permanent magnet synchronous motor based on SVM-DTC," *IEICE Electronics Express*, Vol. 18, No. 1, 20 200 375–20 200 375, 2021.
- [7] Li, Z., F. Wang, D. Ke, J. Li, and W. Zhang, "Robust continuous model predictive speed and current control for PMSM with adaptive integral sliding-mode approach," *IEEE Transactions on Power Electronics*, Vol. 36, No. 12, 14 398–14 408, 2021.

- [8] Yi, P., X. Wang, D. Chen, and Z. Sun, "PMSM current harmonics control technique based on speed adaptive robust control," *IEEE Transactions on Transportation Electrification*, Vol. 8, No. 2, 1794–1806, 2022.
- [9] Nguyen, T. T., H. N. Tran, T. H. Nguyen, and J. W. Jeon, "Recurrent neural network-based robust adaptive model predictive speed control for PMSM with parameter mismatch," *IEEE Transactions on Industrial Electronics*, Vol. 70, No. 6, 6219–6228, 2023.
- [10] Li, X., W. Xu, C. Ye, and I. Boldea, "Comparative study of transversal-flux permanent-magnetic linear oscillatory machines for compressor," *IEEE Transactions on Industrial Electronics*, Vol. 65, No. 9, 7437–7446, Sep. 2018.
- [11] Du, G., W. Xu, J. Zhu, and N. Huang, "Effects of design parameters on the multiphysics performance of high-speed permanent magnet machines," *IEEE Transactions on Industrial Electronics*, Vol. 67, No. 5, 3472–3483, 2020.
- [12] Wang, S., Q. Zhang, D. Wu, and J. Zhao, "Multi-amplitude voltage vector MPTC for dual three-phase PMSMs with low torque ripple," *Journal of Power Electronics*, Vol. 24, No. 1, 68–77, 2024.
- [13] Liu, Q. and K. Hameyer, "High-performance adaptive torque control for an IPMSM with real-time MTPA operation," *IEEE Transactions on Energy Conversion*, Vol. 32, No. 2, 571–581, 2017.
- [14] Di Gennaro, S., J. R. Domínguez, and M. A. Meza, "Sensorless high order sliding mode control of induction motors with core loss," *IEEE Transactions on Industrial Electronics*, Vol. 61, No. 6, 2678–2689, 2014.
- [15] Niu, X., S. Cong, D. Wang, and W. Chen, "Anti-disturbance dynamic surface control for position tracking of interior permanent magnet synchronous motor based on nonlinear extended state observer," *IEEE Access*, Vol. 9, 84 180–84 190, 2021.
- [16] Junejo, A. K., W. Xu, C. Mu, M. M. Ismail, and Y. Liu, "Adaptive speed control of PMSM drive system based a new sliding-mode reaching law," *IEEE Transactions on Power Electronics*, Vol. 35, No. 11, 12 110–12 121, 2020.
- [17] Han, K., M. Choi, B. Lee, and S. B. Choi, "Development of a traction control system using a special type of sliding mode controller for hybrid 4WD vehicles," *IEEE Transactions on Vehicular Technology*, Vol. 67, No. 1, 264–274, Jan. 2018.
- [18] Le, T.-L. and M.-F. Hsieh, "An enhanced direct torque control strategy with composite controller for permanent magnet synchronous motor," *Asian Journal of Control*, 2024.
- [19] Le, T.-L. and M.-F. Hsieh, "A sliding mode-based single-loop control strategy for permanent magnet synchronous motor drives," *IET Power Electronics*, Vol. 17, No. 1, 78–91, 2024.
- [20] Yang, F., X. Zhao, H. Jin, X. Wang, and X. Liu, "Improved dead-beat predictive current control with embedded resonant polynomial and disturbance observer for PMSM current distortion rejection," *IEEE Journal of Emerging and Selected Topics in Power Electronics*, 2024.
- [21] Han, J., "A class of extended state observers for uncertain systems," *Control and Decision*, Vol. 10, No. 1, 85–88, 1995.
- [22] Han, J., "From PID to active disturbance rejection control," *IEEE Transactions on Industrial Electronics*, Vol. 56, No. 3, 900–906, 2009.
- [23] Su, Y. X., B. Y. Duan, C. H. Zheng, Y. F. Zhang, G. D. Chen, and J. W. Mi, "Disturbance-rejection high-precision motion control of a Stewart platform," *IEEE Transactions on Control Systems Technology*, Vol. 12, No. 3, 364–374, 2004.
- [24] Zheng, Q., L. Dong, D. H. Lee, and Z. Gao, "Active disturbance rejection control for MEMS gyroscopes," in *2008 American Control Conference*, 4425–4430, IEEE, 2008.
- [25] Zheng, Q., L. Q. Gao, and Z. Gao, "On validation of extended state observer through analysis and experimentation," *J. Dyn. Sys., Meas., Control.*, Vol. 134, No. 2, 024505, 2012.
- [26] Guo, B.-Z. and Z.-I. Zhao, "On the convergence of an extended state observer for nonlinear systems with uncertainty," *Systems & Control Letters*, Vol. 60, No. 6, 420–430, 2011.
- [27] Xiao, Q., Z. Tang, W. Zhang, Z. Yu, and Z. Cheng, "A robust model predictive current control strategy with low complexity for PMSM," *Progress In Electromagnetics Research C*, Vol. 136, 161–174, 2023.
- [28] Liu, J. M., Z. Ge, X. Wu, G. Wu, S. Xiao, and K. Huang, "Predictive current control of permanent magnet synchronous motor based on duty cycle modulation," *Proceedings of the CSEE*, Vol. 40, No. 10, 3319–3328, 2020.
- [29] Zhang, H. Y., H. Y. Li, J. H. Xiong, *et al.*, "Control strategy for permanent magnet synchronous motor with 2-DOF PI control based on ESO," *Electric Machines & Control Application*, Vol. 48, No. 05, 40–45, 2021.